

# Two body relaxation in CDM simulations

Juerg Diemand,<sup>\*</sup> Ben Moore, Joachim Stadel, Stelios Kazantzidis,

*Institute for Theoretical Physics, University of Zürich, CH-8057 Zürich, Switzerland*

2 November 2018

## ABSTRACT

N-body simulations of the hierarchical formation of cosmic structures suffer from the problem that the first objects to form always contain just a few particles. Although relaxation is not an issue for virialised objects containing millions of particles, collisional processes will always dominate within the first structures that collapse. First we quantify how the relaxation varies with resolution, softening, and radius within isolated equilibrium and non-equilibrium cuspy haloes. We then attempt to determine how this numerical effect propagates through a merging hierarchy by measuring the local relaxation rates of each particle throughout the hierarchical formation of a dark matter halo. The central few percent of the final structures - a region which one might naively think is well resolved at the final time since the haloes contains  $\approx 10^6$  particles - suffer from high degrees of relaxation. It is not clear how to interpret the effects of the accumulated relaxation rate, but we argue that it describes a region within which one should be careful about trusting the numerical results. Substructure haloes are most affected by relaxation since they contain few particles at a constant energy for the entire simulation. We show that relaxation will flatten a cusp in just a few mean relaxation times of a halo. We explore the effect of resolution on the degree of relaxation and we find that increasing  $N$  slowly reduces the degree of relaxation  $\propto N^{-0.25}$  rather than proportional to  $N$  as expected from the collisionless Boltzmann equation. Simulated with the same relative mass resolution (i.e. equal numbers of particles) cluster mass objects suffer significantly more relaxation than galaxy mass objects since they form relatively late and therefore more of the particles spend more time in small  $N$  haloes.

**Key words:** methods: N-body simulations – methods: numerical – dark matter — galaxies: haloes

## 1 INTRODUCTION

A standard technique to study the formation and evolution of gravitating systems is to perform an  $N$ -body simulation in which the mass distribution is discretised into a series of softened point particles. This solution can be exact for a star cluster where each particle represents a single star, but for cosmological simulations of the dark matter each particle can be  $10^{70}$  times larger than the GeV mass candidates being simulated. In this approach the particles represent a coarse grained sampling of phase space which sets a mass and spatial resolution. Unfortunately these super-massive particles will undergo two body encounters that lead to energy transfer as the system tends towards equipartition. In the real Universe the dark matter particles are essentially collisionless and pass unperturbed past each other.

The processes of relaxation is difficult to quantify, but in the large  $N$  limit the discreteness effects inherent to the

N-body technique vanish, so one tries to use as large a number of particles as computationally possible. Increasing the mass resolution of a given simulation allows a convergence test of properties such as the dark matter density profile i.e. Moore et al. (1998), Ghigna et al. (2000), Klypin et al. (2001) and Power et al. (2003). These authors find that to resolve the central one per cent of a dark matter halo the entire system must contain of the order a million particles. It is not known what process sets this resolution scale since with one million particles relaxation is expected to be small, even at one per cent of the virial radius.

Unfortunately in most cosmological simulations the importance of two body interactions does not vanish if one increases  $N$ . Structure formation in the cold dark matter (CDM) model occurs hierarchically since there is power on all scales, so the first objects that form in a simulation always contain only a few particles (Moore et al. 2001), (Binney & Knebe 2002). With higher resolution the first structures form earlier and have higher physical densities because they condense out of a denser environment. Two

<sup>\*</sup> diemand@physik.unizh.ch

body relaxation increases with density, so it is not clear if increasing the resolution can diminish the overall amount of two body relaxation in a CDM simulation, i.e. if testing for convergence by increasing the mass resolution is appropriate.

In isolated equilibrium systems relaxation rates can be measured from the energy dispersion. In cosmological simulations one can measure the amount of mass segregation of multi-mass simulations (Binney & Knebe 2002) where lighter particles gain more energy from collisional processes than the heavier particles. In Section 2 we present a Fokker-Planck type relaxation time estimate, which was fitted to a series of test simulations (Section 3.1) where we explore the relaxation rates as a function of  $N$ , radius and softening parameter in both equilibrium and non-equilibrium cuspy haloes. We then use this local relaxation rate estimate to follow the relaxation history of each particle during 1000 time-steps of a hierarchical CDM simulation. The resulting degree of relaxation as a function of spatial position within galaxy and cluster mass haloes is analysed in Section 4 and in Section 5 we discuss the effects that relaxation has on haloes at  $z = 0$ .

## 2 A LOCAL RELAXATION TIME ESTIMATE

In this paper we adopt the energy definition of the relaxation time (Chandrasekhar 1942) stating that the mean relaxation time  $T$  of a group of stars is the time after which the mean square energy change due to successive encounters equals the mean kinetic energy of the group:

$$T = \Delta t \frac{\overline{E_{kin}^2}}{\Delta E^2(\Delta t)}, \quad (1)$$

where  $\Delta E(\Delta t)$  is the energy difference of one particle after time interval  $\Delta t$  and the bar denotes the group average.

Note that this time is half of the relaxation time  $T_v$  defined in Binney & Tremaine (1987) who calculate a mean velocity change, because  $\Delta E^2/E^2 \simeq 2\Delta v^2/v^2$ . The orbit averaged Fokker-Planck estimate for  $T_v$  is

$$T_v = 0.34 \frac{\sigma^3}{G^2 m \rho \ln \Lambda}, \quad \Lambda \equiv \frac{b_{max}}{b_{min}}, \quad (2)$$

where  $\sigma$  is the one dimensional velocity dispersion,  $\rho$  the density and  $m$  the particle mass. The parameters  $b_{min}$  and  $b_{max}$  are the minimum and maximum limits for the impact parameter.

To assess the degree of relaxation in cosmological simulations (section 4) we estimate the local relaxation rate for each particle after every time-step and integrate this up over the whole run:

$$d(t_k) := \sum_{n=1}^k r_{LE}(t_n) \Delta t. \quad (3)$$

For the local relaxation rate we use a formula similar to (2)

$$T_{LE} = \frac{1}{r_{LE}} = \gamma \frac{\sigma^3}{G^2 m \rho C}, \quad \gamma \equiv 0.17. \quad (4)$$

The value of  $\gamma$ , and the parameters in the Coulomb logarithm  $C$  are chosen to roughly fit measured relaxation times of equilibrium haloes, see section (3). The Coulomb logarithm is

$$C \equiv 0.5 \left[ \ln(1 + \Lambda^2) - \frac{\Lambda^2}{1 + \Lambda^2} \right] (\simeq \ln \Lambda, \text{ if } \Lambda \gg 1), \quad (5)$$

the analytical calculation for Newtonian potentials shows that  $b_{min} = b_0 = 2Gm/v_{rel}^2$ ,  $b_0$  is the impact parameter where the deflection angle reaches  $\pi/2$  (Bertin 2000). In a softened potential the scattering calculation has to be done numerically and the results agree roughly with the Newtonian case if one sets  $b_{min} = \epsilon$ , i.e. one ignores all encounters with an impact parameter smaller than the softening length (Theis 1998). We set

$$b_{min} \equiv \max(Gm/3\sigma^2, \epsilon) \simeq \max(b_0, \epsilon), \quad (6)$$

because  $\overline{v_{rel}^2} = 6\sigma^2$ . The proper choice of  $b_{max}$  is controversial, it is not clear whether it should be related to the size of the whole system or to the mean interparticle distance. For cosmological simulations we prefer the second choice

$$b_{max} \equiv \beta(m/\rho)^{1/3} \quad (7)$$

because this is a local quantity that is easy to measure and less ambiguous than defining the size of irregular shaped, collapsing structures.

We calculate the local velocity dispersion and density surrounding each particle by averaging over its 16 nearest neighbours. We do a simple top-hat average, because using an SPH spline kernel leads to biased results when using only 16 particles. We found good agreement with all measured relaxation rates (3) when using  $\beta = 10$  and  $\gamma = 0.17$ . Averaging over different numbers of nearest neighbours the optimal parameters differ slightly due to different amounts of numerical noise in the local density and velocity dispersion.

## 3 TWO BODY RELAXATION IN SPHERICAL HALO MODELS

In this section we present a number of test cases which we used to gauge our local estimate (3) for the degree of relaxation and show that it agrees quite well (within 15 per cent) with measured levels of relaxation for a wide range of particle numbers, softening lengths and virial ratios. This range covers the haloes that form in cosmological simulations, however all the test cases are isotropic, spherical haloes. Haloes in cosmological simulations are close to isotropic, but are triaxial and contain substructures. But one can argue that locally the two are similar, and if a local relaxation time estimate works in the spherical haloes, it should give a reasonable estimate also in the cosmological case.

### 3.1 Equilibrium haloes

In an equilibrium model the energy of each particle would be conserved in the  $N \rightarrow \infty$  limit. For finite  $N$  the energies of particles suffer abrupt changes due to encounters. Therefore we just have to measure these energy differences to get the relaxation time with (1).

Here we present a sequence of tests using spherical and isotropic Hernquist models (Hernquist 1990) which are a reasonable approximation to the haloes found in cosmological  $N$ -body simulations. (We found no difference between these simulations and tests using Navarro, Frenk & White (1996)

and Moore et al. (1999) profiles, constructed by solving for the exact phase space distribution function numerically as described in Kazantzidis, Magorrian & Moore (2003.) The density profile of the Hernquist model is

$$\rho(r) = \frac{M a}{2\pi r} \frac{1}{(r+a)^3}. \quad (8)$$

We set <sup>1</sup> the total mass to  $M = 3.5 \times 10^9 M_\odot$  and the scale length to  $a = 10$  kpc. Then the half mass radius is  $r_h \simeq 2.4a = 24$  kpc and the crossing time at half mass radius is  $T_c \equiv r_h/v_{circ}(r_h) \simeq 1.3$  Gyr.

All the simulations have been carried out using PKDGRAV, a state of the art, multi-stepping, parallel tree-code (Stadel 2001). The time-steps are chosen proportional to the square root of the softening length over the acceleration on each particle,  $\Delta t_i = \eta \sqrt{\epsilon/a_i}$ . We use  $\eta = 0.25$ , and a node-opening angle  $\theta = 0.55$  for all runs in this section, expect the long term integrations in subsection 3.3 where we use  $\eta = 0.03$ . Energy conservation was better than 0.1 per cent after several crossing times for all runs in this section.

Due to softening the initial models are not exactly in equilibrium, the total kinetic energy is a few percent larger than half of the potential energy. For this reason we evolved the models for five crossing times before measuring the energy dispersion, which results in up to 10 per cent longer relaxation times.

Figure 1 shows  $\overline{\Delta E^2(\Delta t)}$  as a function of time within haloes constructed with  $N = 10^4$  and  $N = 100$  particles. The upper panel shows that for small numbers of particles  $N \ll 10^3$   $\Delta E(\Delta t)$  becomes very noisy since there are fewer, but more significant encounters. To obtain more reliable results in small  $N$  groups we added a sufficiently large number ( $10^4$ ) of massless tracer particles following the same distribution in real and velocity space as the massive particles. The open squares in Figure 1 show the 'energy' dispersion of the tracers, which in large  $N$  groups is just the same as the energy dispersion of the massive particles, but it evolves much smoother with time in small  $N$  groups. We obtain the mean relaxation times (1) of these haloes with linear fits to the energy dispersion of the tracer particles (open squares), taking into account points where  $\overline{\Delta E^2} < 0.2$ , i.e. in the upper panel only the points left of the vertical bar, to make sure that  $\Delta t$  is small compared to the relaxation time. The local relaxation estimate (solid line) (4) gives similar average degrees of relaxation in these test cases (see also Figures 2 and 3).

Note that the tracers are not in equilibrium with the halo, on average they gain speed in encounters and are ejected from the core. Typically after one relaxation time the number of tracers inside of  $r = a$  drops to one half of the initial number. Therefore it is important to use a  $\Delta t$  shorter than  $T$  and to add the tracers after evolving the halo for five crossing times, otherwise the relaxation in the core is not sufficiently reflected in the energy dispersion of the tracers and  $T$  could be underestimated significantly.

<sup>1</sup> To rescale the results to different size haloes just change the distance scale by some factor  $x \rightarrow fx$ , mass scale  $M \rightarrow f^3 M$  and the dynamical and relaxation timescales do not change. To rescale to different timescales  $T \rightarrow cT$  do  $M \rightarrow c^{-2} M$  with fixed length scale.

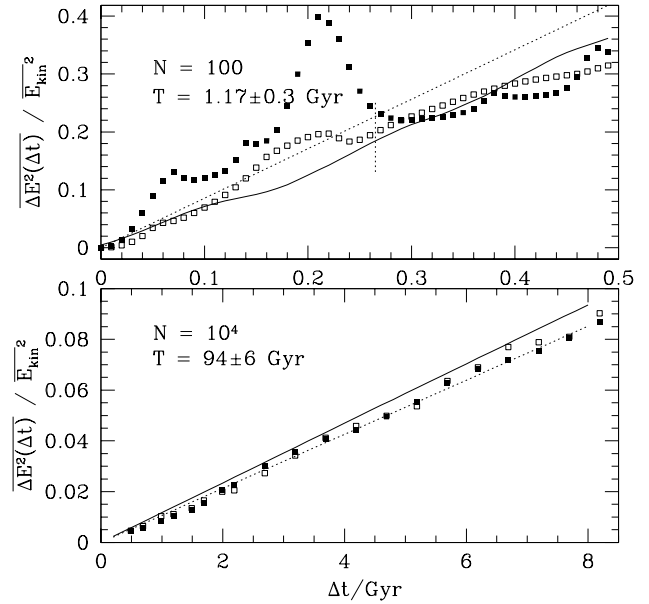


**Figure 1.** Mean squared energy change  $\overline{\Delta E^2(\Delta t)}$  as a function of time. The filled squares show the mean squared energy change of the actual particles, the open squares for the massless tracer particles. The dotted lines are linear fits to the mean squared energy change of the tracers, in the upper panel only the points left of the vertical bar are taken into account. The solid lines are averages of (3) over all massive particles.

### 3.1.1 Dependence on $N$ and $\epsilon$

Figures 2 and 3 show the measured mean relaxation times as a function of  $N$  and softening parameter,  $\epsilon$ , compared with the average over all particles of the local relaxation estimate (4). We find that the measured relaxation times are proportional to  $N$  (dashed reference line), rather than to  $N/\ln(N)$  (dotted line), as expected for a softened potential. The same result was found for King models by Huang, Dubinski & Carlberg (1993). The local estimate of the relaxation time increases slightly faster with  $N$  than the measured values. This is due to the fact that we choose a maximum impact parameter proportional to the mean interparticle separation, i.e.  $b_{max} \propto N^{-1/3}$ , but the difference is less than 10 per cent for all relaxation times shorter than a Hubble time, i.e. for  $N \leq 10^4$ .

The dependence on the softening length is shown in Figure 3 for a  $N = 10^4$  model. The measured values (filled squares) increase faster with  $\epsilon$  than the local estimate (open squares) (like in Figure 2 of Huang et al. 1993), but the differences are small ( $\gtrsim 15$  per cent) for realistic softenings  $\epsilon \lesssim 0.1a = 1$  kpc. The average relaxation time of this model increases from 30 Gyr to 180 Gyr when the softening parameter is changed from 0.01 kpc to 1 kpc. This is slightly higher than expected from the scaling with  $\ln(\epsilon)$  since the density profile and central cusp are better resolved with smaller softening.

### 3.1.2 Dependence on radius

Measuring the relaxation time as a function of radius  $T(r)$  proved to be quite difficult. The most credible method seems

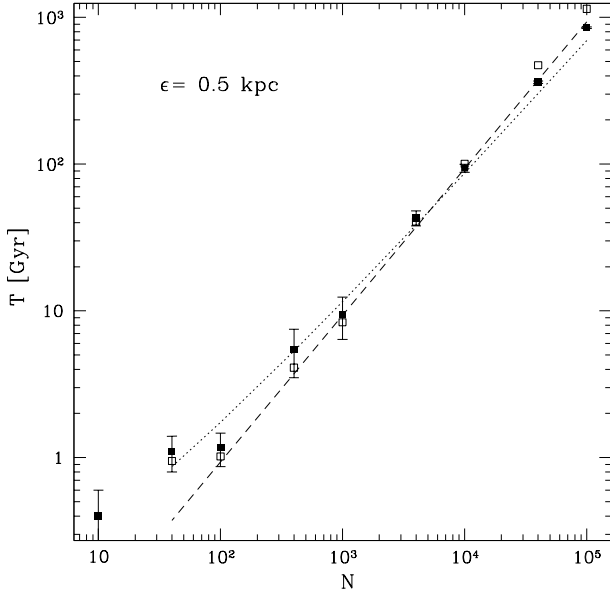


**Figure 2.** Average relaxation times of isotropic Hernquist models versus particle number  $N$ , with a constant softening  $\epsilon = 0.5$  kpc. The filled squares are the measured relaxation times, with error bars form the linear fit of  $\overline{\Delta E^2}(\Delta t)$ . The open squares are the local estimates of the relaxation time (4).

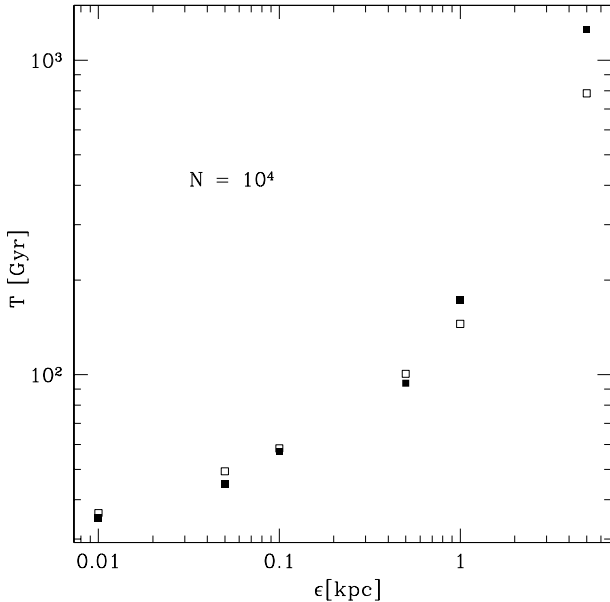


**Figure 3.** Average relaxation times of an  $N = 10^4$  Hernquist models versus softening length  $\epsilon$ . The filled squares are the measured relaxation times, the open squares are the local estimate (4).

to take (1) and replace the average over all particles by the average over those which are in the corresponding radial bin at the beginning (or at the end) of the time interval  $\Delta t$ . Clearly one has to choose  $\Delta t \ll \delta r / \sigma(r)$ , where  $\delta r$  is the size of the bins, to make sure that most particles spend most of  $\Delta t$  in the same bin. This could also be achieved by placing the tracers on circular orbits, which leads to very similar

results for  $T(r)$  if  $r \sim r_h$ , but in to the centre this method fails, because there the circular velocity is much smaller than the velocity dispersion<sup>2</sup>.

In Figure (4) we plot the relaxation rate against radius for a Hernquist model with  $10^4$  particles. We measured the energy dispersion (filled squares) during  $\Delta t = 0.1$  Gyr for each particle, and averaged the values of particles starting in the same radial bin. We also measured the local relaxation rate  $r_{LE}$  (4) at 100 time-steps during  $\Delta t$  for each particle and summed them up. The radial averages are plotted with open squares. Again the agreement with the measured energy changes is better than 35 per cent except in the last three bins where the relaxation rates are many thousands of Gyrs and the local relaxation measurement overestimates the true rate of relaxation. In the inner three bins the crossing times are shorter than 0.2 Gyr, i.e. many of the particles had time to move through these bins during  $\Delta t = 0.1$  Gyr.

The dashed line is the inverse of half the Fokker-Planck estimate (2) with  $\Lambda = r_h / \epsilon$ , calculated using all particles in the bin, not only from 16 nearest neighbours. It scales like the phase space density  $\rho(r) / \sigma^3(r)$  which scales almost exactly like  $r^{-2}$  in a Hernquist model. The local estimate also follows this  $r^{-2}$  scaling in the seven outer bins. The measured relaxation scales more like  $\propto r^{-3}$  in the outer region, but the slope depends strongly on  $\Delta t$ , i.e. on how many particles from the core with 100 times higher relaxation rate have had time to reach the outer region.

The average relaxation times<sup>3</sup> are about 10 times shorter than measured relaxation times at half mass radius, due to the fast relaxation in the high density core of cuspy haloes. For a less concentrated King model ( $\Psi_0 = 5$ ) the Fokker-Planck estimate seems to agree not only with the measured relaxation time at half mass radius, but also with the mean relaxation time (Huang et al. 1993).

### 3.2 Non-equilibrium systems

The definition of the relaxation time (1) is mostly used for systems close to dynamical equilibrium like globular clusters, i.e. systems with constant (or only slowly changing) mean kinetic energy. In this case the mean relaxation rate is also (roughly) constant and the degree of relaxation grows linear with time (like in Figure 1). Generalising this definition to non-equilibrium situations is straightforward: The degree of relaxation of a group at some given time is the accumulated mean square energy change due to encounters divided by the mean square kinetic energy at this time.

Now not all energy changes are due to encounters, so

<sup>2</sup> From a convolution of the velocity distributions one finds that the relative velocities in encounters with tracers on circular orbits have a different dispersion ( $\sigma_{v_{rel}}^2 = 3\sigma^2 + v_{circ}^2$ ) than those of encounters between the massive particles ( $\sigma_{v_{rel}}^2 = 6\sigma^2$ ). In non isothermal haloes,  $3\sigma^2 \neq v_{circ}^2$  and this leads to systematic errors in the measured relaxation times. In Hernquist models  $3\sigma^2 \sim v_{circ}^2$  holds only for  $r \sim r_h$ , and indeed we found good agreement with the other methods only in this range.

<sup>3</sup> Note that analytically the average of the relaxation rate estimate  $r_{LE}$  (2) is divergent for models with central cusps  $\propto r^{-1}$  and steeper:  $T = \int_0^R r_{LE}(r) \rho(r) r^2 dr \propto \int_0^R r^{-2} \rho(r) r^2 dr = \int_0^R \rho(r) dr$ .

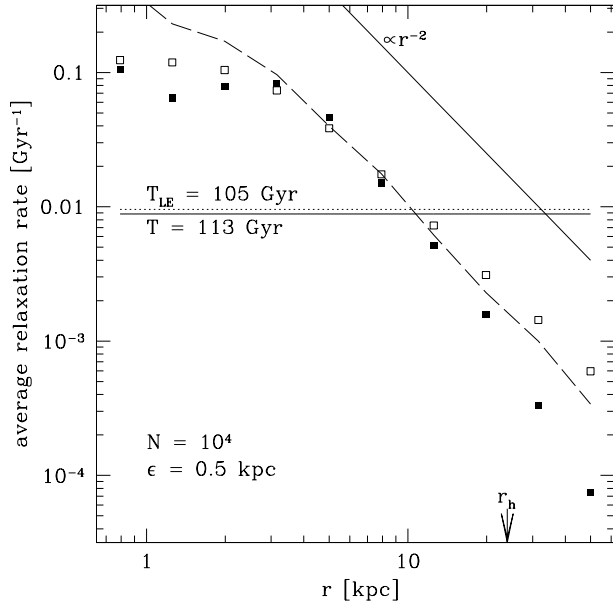


**Figure 4.** Relaxation rate of an  $N = 10^4$  halo vs. radius. The filled squares are the measured relaxation, the open squares are the local estimate  $r_{LE}$ , calculated from 16 nearest neighbours during 0.1 Gyr. The horizontal lines give the halo averages of measured (solid line) and estimated (dotted line) relaxation rates. We also plot  $2/T_v$  (dashed line) calculated from all particles in the radial bin.

one needs another method to measure the degree of relaxation. Again we use massless tracer particles like in the last section. Instead of setting up their initial conditions exactly like those of the massive particles, one can also restrict the tracers to a common orbital plane. In a spherical system this does not change their density profile nor the relative velocities in encounters with the massive particles. If we choose the orbital plane of the tracers to be the  $xy$ -plane, then the accumulated energy change due to encounters  $\Delta_{enc}E$  is

$$\frac{\overline{\Delta_{enc}E(t)^2}}{E_{kin}(t)^2} \simeq \frac{\overline{\Delta_{enc}E_{kin}(t)^2}}{E_{kin}(t)^2} \simeq 2 \frac{\overline{\Delta_{enc}v(t)^2}}{v(t)^2} = 4 \frac{\overline{v_z(t)^2}}{v(t)^2}, \quad (9)$$

as long as  $v_z(t)^2 \ll v(t)^2$ , i.e. for small degrees of relaxation. This relates the energy dispersion to a more demonstrative quantity and in the edge on view of the  $xy$ -plane one can actually observe the relaxation process since the degree of relaxation is roughly proportional to the thickness of the disk<sup>4</sup>. When the amount of relaxation approaches unity (9) tends to underestimate the degree of relaxation, because tracers on new out of plane orbits will eventually reach a turnaround point where  $v_z = 0$ . Also the probability that one tracer suffers more than one encounter grows with time, therefore one should place a new set of tracers into the plane to get an accurate relaxation rate as soon as the amount of relaxation is close to unity.

With (9) we can measure the amount of relaxation in non-equilibrium situations, we only need one symmetry plane to be able to apply this method, therefore it allows us

<sup>4</sup> Simulation movies are available at: [www-theorie.physik.unizh.ch/~diemand/tbr/](http://www-theorie.physik.unizh.ch/~diemand/tbr/)

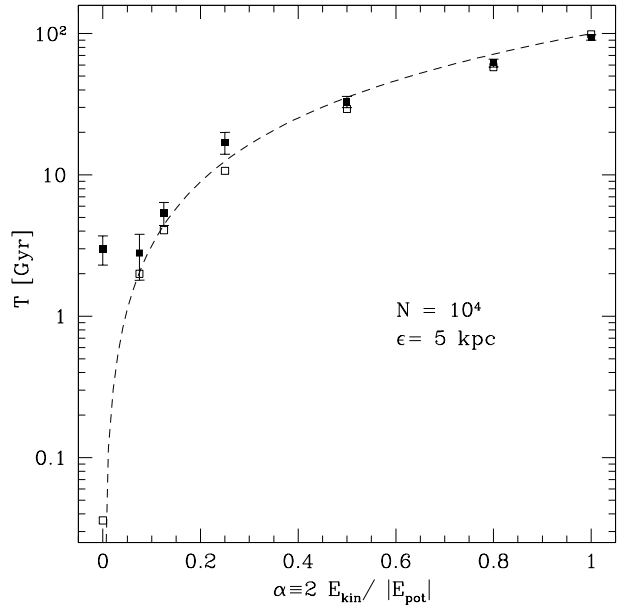


**Figure 5.** Relaxation times of a  $N = 10^4$  non-equilibrium Hernquist model vs. virial ratio. The filled squares are measured with  $v_z^2/\bar{v}^2$ , the open squares are the local estimate (4). The reference line is  $\propto \alpha^{1.5} \propto v^3/\rho$ .

to measure the amount of relaxation during a collapse or a merger.

### 3.2.1 Collapsing haloes

In CDM simulations the virial ratio  $\alpha \equiv 2E_{kin}/|E_{pot}|$  is close to zero at the beginning of a halo collapse and grows towards unity as the halo reaches dynamical equilibrium. In the previous sections we showed that the local estimate (4) works for  $\alpha = 1$ , but for  $\alpha \rightarrow 0$  the phase space density  $\propto \alpha^{-1.5}$  goes to infinity. Down to which virial ratio can we trust our local estimate?

To answer this question we began with equilibrium Hernquist models (same parameters as in section 3.1.1) with  $10^4$  particles and multiplied all velocities with  $\sqrt{\alpha}$ . Therefore  $\sigma^3 \propto \alpha^{1.5}$  and the phase space density  $\rho/\sigma^3 \propto \alpha^{-1.5}$ . To these models we added  $10^4$  massless tracer particles with the same phase-space distribution and tilted their orbital planes into the  $xy$ -plane. Then we measure  $v_z^2/\bar{v}^2$  and the local estimate (4) at 100 time-steps during the first 0.1 Gyr of the collapse. Linear fits give the relaxation times plotted in Figure (5), the dashed line shows the scaling  $\propto \alpha^{1.5}$  expected from the Fokker-Planck type estimates (2) and (4), since these times are proportional to one over phase-space density. Our relaxation time estimate becomes very small when the virial ratio goes to zero, but the measured relaxation times remain on the order of a few dynamical times.  $T_{LE}$  is within a factor of two for  $\alpha \gtrsim 0.075$  and within 10 per cent for  $\alpha \gtrsim 0.5$ . Also after the first 0.1 Gyr the local estimate follows the measured values, one example ( $\alpha = 0.25$ ) is plotted in the top panel of Figure (6).

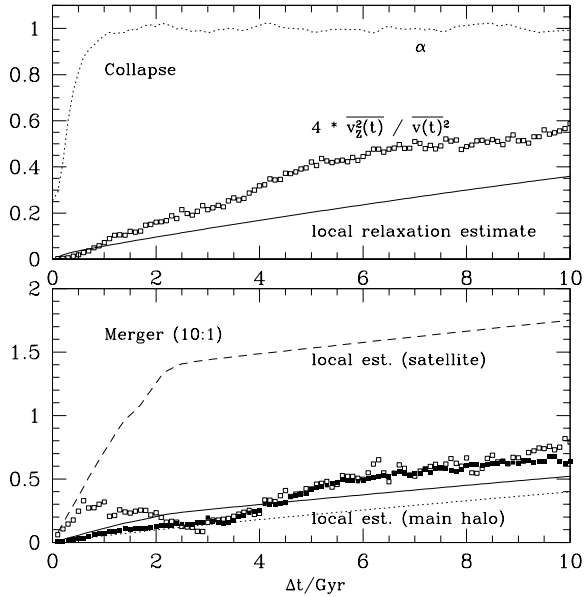


**Figure 6.** Average degrees of relaxation during a collapse of an  $N = 10^4$  Hernquist halo, the initial virial ratio  $\alpha$  is 0.25 (top). The lines are the average of the local relaxation estimate (4), the squares are the amount of relaxation measured from a group of tracer set in a plane initially (9). The bottom panel shows average degrees of relaxation during a merger of an  $N = 10^3$  halo into a ten times more massive system with  $N = 10^4$ . Here the open squares are the measured average for the satellite and the filled squares for the main halo.

### 3.2.2 Mergers

The last test case for the local relaxation estimate is a merger of a small system into a more massive one. The problem in this case is that the small halo gains a lot of kinetic energy when falling into the main halo, so its accumulated energy changes due to encounters can become smaller *relative* to the mean kinetic energy of the group. A local estimate can never capture this decrease since it can not know about the gain in external kinetic energy. For a surviving subhalo one can argue that its accumulated energy changes should still be compared to its roughly constant internal kinetic energy to get an estimate of how affected it is by relaxation. But for haloes that are disrupted (and stripped particles from subhaloes) one has to worry about how their overestimated degrees of relaxation affect the average relaxation of the main halo.

The bottom panel of Figure (6) shows how relaxation develops in a head on merger of a  $N = 10^3$ ,  $a = 3$  kpc halo into a ten times more massive halo with  $N = 10^4$  and  $a = 10$  kpc. The initial separation was 100 kpc with a small relative velocity of 2.2 km/s. The satellite falls in and reaches the centre of the main halo after 3 Gyr. Note how the relaxation of the satellite (open squares) *decreases* during infall, this can not be followed by the average local estimate (4) of the satellite (dashed line), but still the average over the whole system (solid line) gives a good estimate for the mean degree of relaxation. We also verified this for equal mass mergers, there the decrease during infall is small because both haloes have quite large internal energies initially.

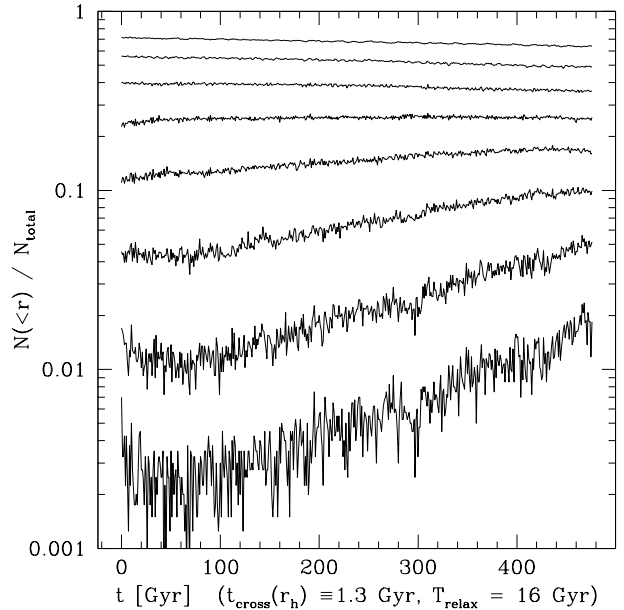


**Figure 7.** From top to bottom, the mass fraction within 0.89, 1.58, 2.81, 5.00, 8.90, 15.8, 28.1 and 50.0 kpc of a  $N = 4'000$  Hernquist models vs. time.

### 3.3 Evolution of isolated Halos

The dynamical evolution of globular clusters is driven by relaxation, which can lead to core collapse and evaporation on a timescale of a few tens of half mass relaxation times, i.e. the core loses energy to an expanding outer envelope of stars and gets denser and hotter (Binney & Tremaine 1987; Spitzer 1987).

In the next section we show that haloes in cosmological simulations are typically between one and ten mean relaxation times old. (In terms of the much longer half mass relaxation time they are younger than one or two half mass relaxation times.) Therefore we do not expect that density profiles in cosmological simulations are significantly affected by the core collapse process.

Studies of globular cluster evolution start with models that are isothermal in the centre (e.g. Plummer spheres, King models) and then show a slow but monotonic density increase in the core. In contrast the cuspy haloes in cosmological simulations are not isothermal: the velocity dispersion decreases in the central regions. In this case relaxation leads to an energy flow inwards, the core evolves towards a less dense, isothermal state first. Later the system evolves just like the models in globular cluster calculations (Quinlan 1996). The N-body simulations of Hayashi et al. (2003) show this evolution starting from an NFW profile. We confirmed their result by evolving an  $N = 4'000$  Hernquist model for 360 crossing times (see Figure 7).

Figure 8 shows the evolution of five  $N = 4'000$  Hernquist models during 16 Gyr, using a softening of  $\epsilon = 0.1$  kpc. For this long term evolution we use a more conservative time step parameter  $\eta = 0.03$ , energy is conserved within 0.36 per cent even after 360 crossing times. The crossing time at the half mass radius is 1.3 Gyr, the initial mean relaxation time is 16 Gyr and the initial half mass relaxation time is 71 Gyr. After 50 Gyr this halo is about three mean relaxation

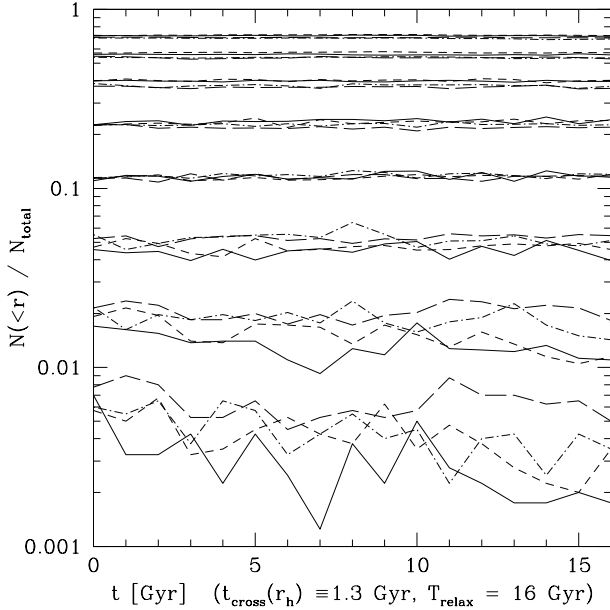


**Figure 8.** From top to bottom, the mass fraction within 0.89, 1.58, 2.81, 5.00, 8.90, 15.8, 28.1 and 50.0 kpc of five  $N = 4'000$  Hernquist models vs. time.

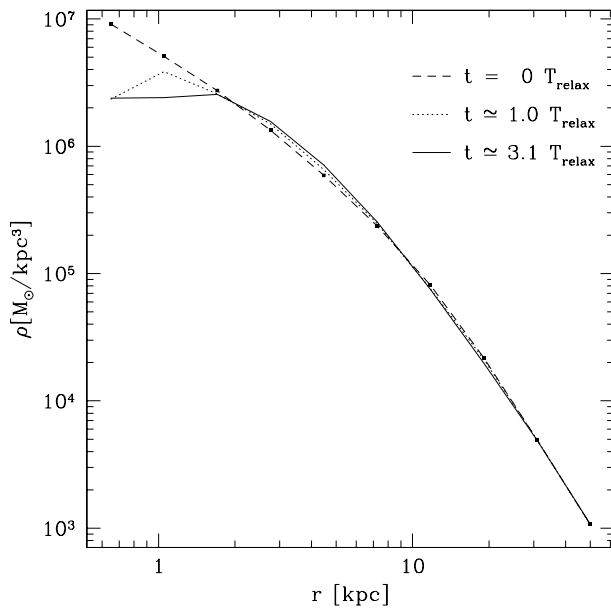


**Figure 9.** Averaged density profiles of five  $N = 4'000$  Hernquist models (same models as in Figure 8), initial profile (dashed line), after 16 Gyr (dotted line) and after 50 Gyr (solid line). The points indicate the radius of the outer borders of the spherical bins.

times old, a realistic value for haloes in current cosmological simulations, see section (4). The same would happen to a  $N = 100$  halo in only 1.25 Gyr, we use  $N = 4'000$  just to have a well defined density profile down to  $0.1a = 1$  kpc.

Within few mean relaxation times the velocity dispersion rises in the centre and at the scale radius it drops slightly, in the end the core is already close to isothermal. This energy gain is compensated with core expansion, the inner two mass shells plotted in Figure 8 clearly lose mass.

This is not a numerical artifact, the softening we used is much smaller than the inner bin and in a  $N = 4 \times 10^4$  reference model the mass loss in the inner two bins is about ten times slower, i.e. this is really an effect driven by relaxation. The corresponding density profiles are less steep in the inner 3 per cent of the halo, see Figure 9, and show constant density cores in this region.

#### 4 RELAXATION IN COSMOLOGICAL SIMULATIONS

Here we present results from four low to medium resolution  $\Lambda$ CDM simulations ( $\Omega_\Lambda = 0.7$ ,  $\Omega_m = 0.3$ ,  $\sigma_8 = 1.0$ ). We generate initial conditions with the GRAFIC2 package (Bertschinger 2001). We start with a  $128^3$  particle cubic grid with a comoving cube size of 60Mpc (particle mass  $m_p = 3.6 \times 10^9 M_\odot$ ). Later we refined two interesting regions, in the first one a cluster halo ( $M_{200} = 7.4 \times 10^{13} M_\odot$ ,  $r_{200} = 1440$  kpc) forms, the refinement factors are 2 and 3 in length, i.e. 8 and 27 in mass (run C2,C3). In the second region a galaxy size halo ( $M_{200} = 1.4 \times 10^{12} M_\odot$ ,  $r_{200} = 350$  kpc) forms. There we used a refinement of 9 in length, i.e. 729 in mass, and included a buffer region, about 2 Mpc deep, with an intermediate refinement factor of 3 (run G9). We start the simulations when the standard deviation of the density fluctuations in the refined region reaches 0.2. The softenings used in the refined regions are  $\epsilon = 1.86$  kpc for the cluster and  $\epsilon = 0.5$  kpc for the galaxy, i.e.  $\epsilon \simeq 0.0013 r_{vir}$  in both cases. We also run the unrefined cube again with this softening in the cluster forming region (run C0). The numerical parameters are as in section 3.1, but at late epochs we use a larger node-opening angle to speedup the runs,  $\theta = 0.7$  for  $z < 2$ .

In non equilibrium, non spherical haloes of a cosmological simulation it is not possible to measure two body relaxation times with the methods used in section 3. Binney & Knebe (2002) used initial conditions with two species of particles with different mass. Both species start from a regular lattice, such that the nodes of one grid are at the centres of the cells of the other, and both are then displaced according to the Zel'dovich approximation. In a collisionless simulation the final distribution of the particles would be independent of mass. They found differences in the number density of the light and heavy particles in the centres of haloes.

Here we compliment the study of Binney & Knebe by applying the results of the previous sections to cosmological simulations. We assign a degree of relaxation  $d$  to each particle, which is calculated after each of 1000 fixed time-steps  $\Delta t$  from the local relaxation rate estimate (4) and summed up over the whole cosmological simulation (3).

As shown in section 3.2.1,  $r_{LE}$  reflects the measured relaxation rates only for virial ratios  $\alpha \gtrsim 0.1$ . Since this is not case for the first steps in a CDM simulation, we set  $r_{LE}$  to zero before the local density reaches some threshold. When the local density reaches  $6\rho_0$  ( $\simeq$  density at turnaround in the spherical collapse) the typical values for  $\alpha$  are close to 0.4, later at  $170\rho_0$  ( $\simeq$  density at virialisation in the spherical collapse)  $\alpha$  is close to unity. We used these two density thresholds, in the first case we write  $d_{TA}$  for the ‘‘degree of relaxation since turnaround’’, otherwise  $d_{VIR}$  for ‘‘degree of

**Table 1.** Average Degrees of Relaxation

| Run                           | C0     | C2      | C3      | G9      |
|-------------------------------|--------|---------|---------|---------|
| $N_{200}$                     | 20'500 | 177'000 | 650'000 | 250'000 |
| $d_0$ inside $0.1r_{200}$     | 5.98   | 3.62    | 3.06    | 1.67    |
| $d_0$ inside $r_{200}$        | 5.23   | 3.34    | 2.52    | 1.15    |
| $d_{TA}$ inside $0.1r_{200}$  | 4.74   | 2.40    | 1.78    | 0.72    |
| $d_{TA}$ inside $r_{200}$     | 3.67   | 2.42    | 2.12    | 1.02    |
| $d_{VIR}$ inside $0.1r_{200}$ | 3.58   | 1.61    | 1.17    | 0.42    |
| $d_{VIR}$ inside $r_{200}$    | 2.50   | 1.52    | 1.34    | 0.58    |

relaxation since virialisation”. The relaxation averages over all particles inside  $r_{200}$  and  $0.1r_{200}$  at  $z = 0$  are given in table 1.

#### 4.1 Number of particles

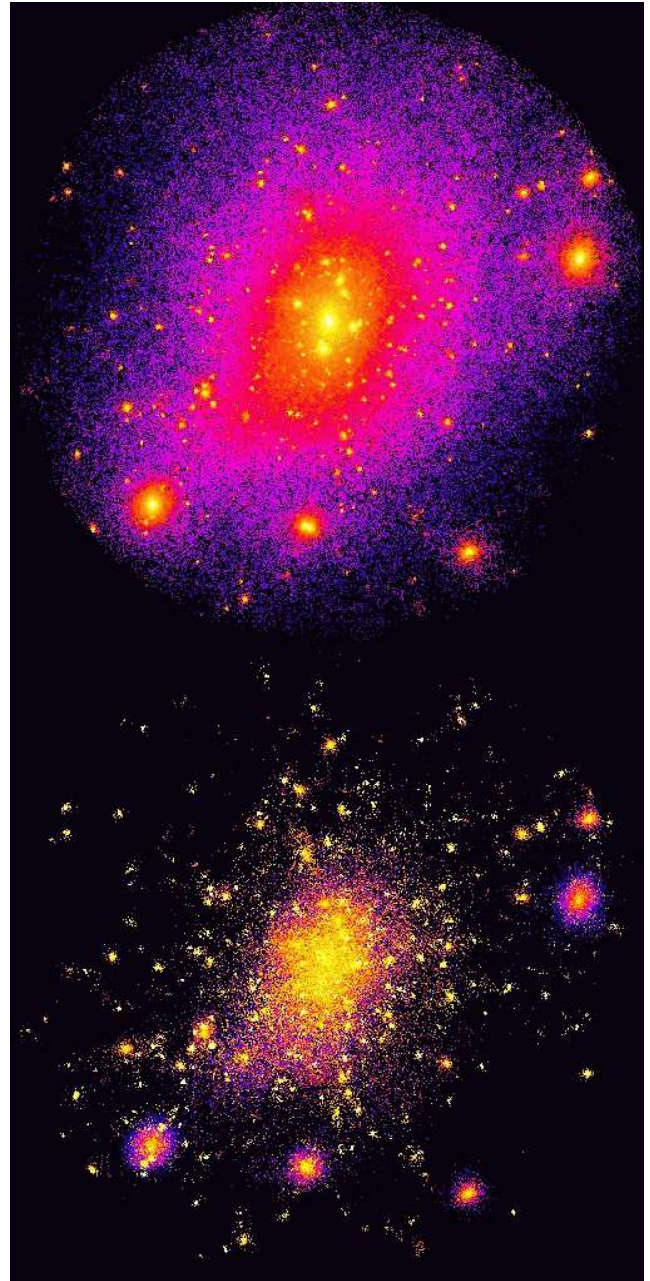
A reassuring result is that with more particles the simulations are less affected by two-body relaxation, even though one resolves more small  $N$  progenitors. This confirms the significance of convergence tests that vary the number of particles. The average degree of relaxation inside of  $0.1r_{200}$  scales like  $N^{-0.3}$ , and the relaxation inside of  $r_{200}$  like  $N^{-0.2}$ .

Figure 11 shows the relaxation in the cluster as a function of the final particles position, for three different resolutions. In the outer part ( $r \gtrsim 0.1r_{200}$ ) the cluster has substructure, which are small  $N$  systems that exist at the present time, so they are still relaxing at a high rate at  $z = 0$  (bottom panel). Substructure haloes with  $N \simeq 500$  can reach averages of  $d_{VIR} \simeq 10$  in all runs, the highest peaks in  $d_{VIR}$  are found in the centre of substructure haloes, where  $d_{VIR}$  can be as high as 100, much higher than in the centre of the host halo (see Figure 10).

Note that the degrees of relaxation (top and middle panel) are much larger than what you would estimate using the final distribution of particles (bottom panel). Other studies consider only the relaxation rate at  $z = 0$ , and claim to resolve a halo down to a radius where this relaxation time  $r_{LE}^{-1}(z = 0)$  is larger than Hubble time (Power et al. 2003) or larger than three Hubble times (Fukushige & Makino 2001). This radius scales  $\propto N^{-0.5}$ , whereas convergence in N-body simulations seem to be slower; In Moore et al. (1998) and Ghigna et al. (2000) the resolved radii are determined by comparing density profiles between simulations with different numbers of particles. They found that the “resolved radius”  $r \simeq 0.5(N_{200}/V_{200})^{-1/3}$  for a wide range of  $N_{200}$  from  $10^2$  to  $10^{5.7}$ . It appears like the resolved radius scales in the same way as the average degree of relaxation, but further relaxation studies for a wider range  $N$  are needed to verify this.

#### 4.2 Mass and time dependence

Figure 12 compares the relaxation rate within the high resolution cluster and the galaxy simulations. The average degree of relaxation at  $z = 0$  for the galaxy ( $d_{VIR} \simeq 0.58$ ) is much smaller than for the cluster ( $d_{VIR} \simeq 1.34$ ), even though  $N$  is larger for the cluster and therefore the present relaxation rate  $r_{LE}(z = 0)$  is smaller in the cluster. The



**Figure 10.** Maps of the cluster’s density (top) and relaxation since virialisation (bottom) out to  $r_{200}$  for the C3 run ( $N_{200} \simeq 650'000$ ). The logarithmic scale for the degree of relaxation goes from 0.01 (black) to 100 (white).

reason is that the cluster forms much later than the galaxy therefore most of its particles have spent a longer period of time in small  $N$  progenitor haloes.

In Figures 13 and 14 we plot how the degree of relaxation increases with time for both haloes for particles within 10 per cent of the virial radius and for all the particles within the virial radius. Most of the relaxation within the central region of the galaxy occurs within the first couple of Gyrs of the evolution of the Universe. The cluster forms over a longer timescale and this is reflected in the longer increase in the degree of relaxation with time.

The cluster runs (C0,C2,C3) show how relaxation in small  $N$  groups starts earlier, after 1 Gyr the highest reso-



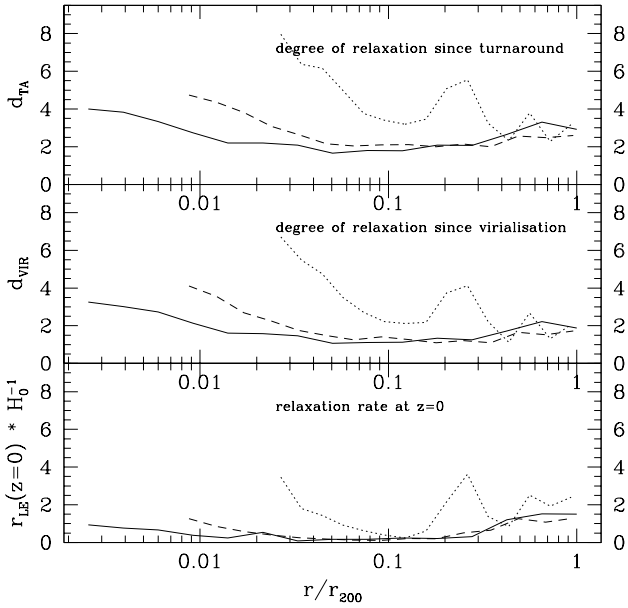


**Figure 11.** Relaxation versus radius. The solid line is for run C3, the dashed line for run C2 and the dotted line for run C0.

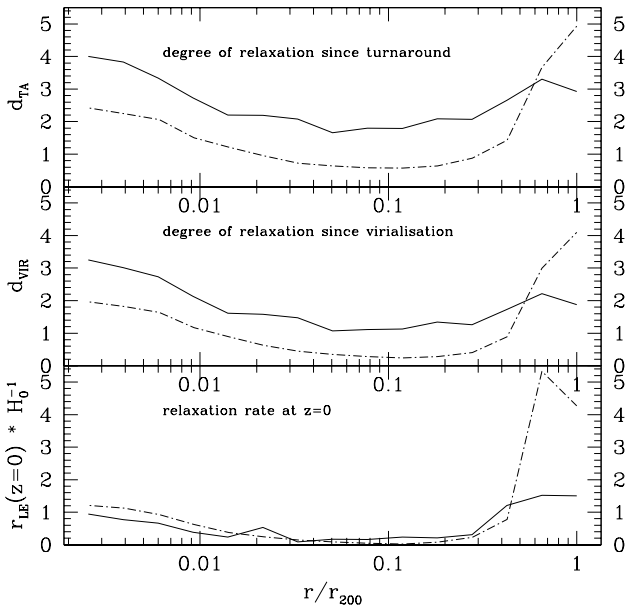


**Figure 12.** Relaxation vs. radius. The solid line is the cluster run C3 ( $N_{vir} \simeq 650'000$ ), the dot - dashed line for the galaxy ( $N_{vir} \simeq 250'000$ ).

lution run (C3) is most affected by relaxation. This result is not an artifact from using a density threshold, we checked that the  $d_0$  shows the same behaviour as  $d_{VIR}$ . The entire haloes (bottom panel) show some relaxation during the whole simulation which arises from the poorly resolved substructure haloes in the outer regions.

## 5 CONCLUSIONS AND DISCUSSION

$N$ -body cosmological simulations attempt to model a collisionless system of particles using a technique that is in-

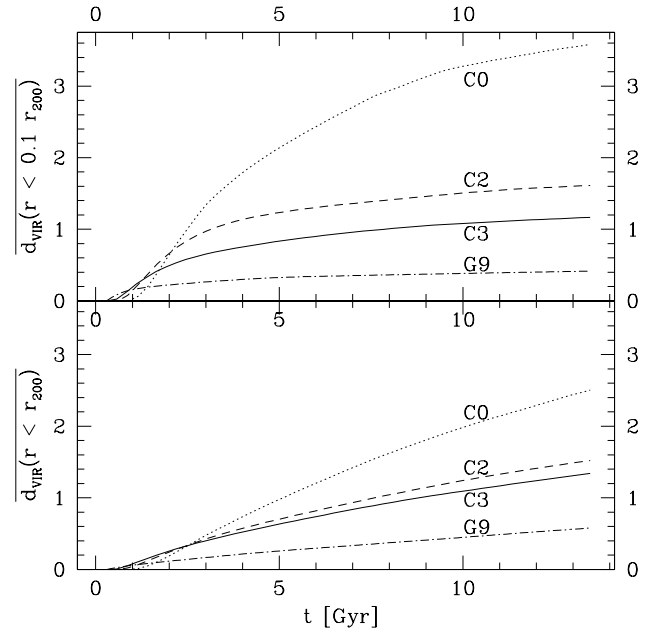


**Figure 13.** The degree of relaxation,  $d_{VIR}$ , averaged over all particles as a function of time. In the top panel we average over particles inside  $0.1 r_{200}$  at  $z = 0$  and in the bottom panel over all inside  $r_{200}$ .

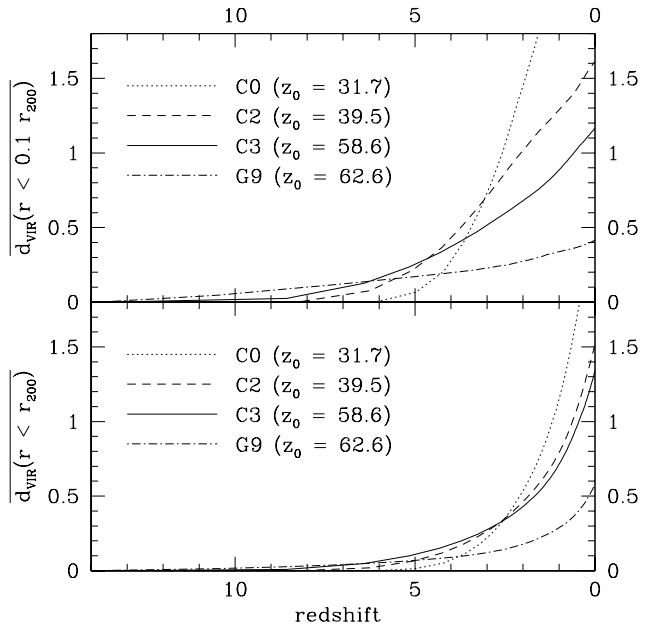


**Figure 14.** Same as Figure 13 but as a function of redshift.  $z_0$  is the starting redshift of the runs.

herently collisional on small scales. We have examined the relaxation rates of isolated equilibrium cuspy haloes as a function of particle number, radius and softening parameter. Our results apply primarily to  $n$ -body,  $P^3M$  codes, such as direct or treecodes. Adaptive grid based methods, such as ART (Kravtsov, Klypin & Khokhlov 1997) and MLAPM (Knebe, Green & Binney 2001) also seem to suffer from relaxation but at slightly lower rates than from those quantified here (Binney & Knebe 2002).

We show how one can define a local relaxation timescale

for each particle by measuring its local phase space density which we applied to cosmological simulations in an attempt to determine the regions most affected by numerical relaxation. We summarise our results here:

(i) The relaxation rates in cuspy dark matter haloes are in good agreement with the rates predicted by the orbit averaged Fokker-Planck equation. However the average relaxation time is an order of magnitude less than that measured at the half mass radius.

(ii) We verify that the average relaxation time of a halo is proportional to the number of particles it contains and to the inverse natural logarithm of the softening parameter.

(iii) The relaxation time is proportional to the local phase space density which allows us to measure the cumulative amount of relaxation each particle undergoes during the evolution of a halo.

(iv) We show that we can measure the relaxation rate in collapsing or non-equilibrium haloes that have kinetic to potential energy ratios up to ten times smaller than the equilibrium value.

(v) Averaging over several simulations of cuspy Hernquist haloes we show that within few mean relaxation times the central cusp is transformed into a constant density core.

(vi) We show that the hierarchical build up of galaxy or cluster mass haloes leads to a greatly enhanced degree of relaxation within their central regions. The substructure haloes suffer from the highest rates of relaxation since they contain the fewest particles for the longest period of time. Subhaloes are typically several relaxation times old therefore one should be cautious about interpreting their internal structure using simulations of order  $10^6$  particles (Stoehr et. al 2002).

(vii) Cluster haloes suffer three times the amount of relaxation as galaxy haloes simulated at the same relative spatial and mass resolution. This is because the cluster forms later and more of its particles spend time in poorly resolved progenitors.

(viii) Increasing the resolution ( $N$ ) at a fixed force softening reduces the the accumulated amount of relaxation. The average degree of relaxation in CDM haloes at  $z = 0$  scales  $\propto N^{-0.2}$ , in the inner 10 percent  $\propto N^{-0.3}$ . Relaxation may therefore provide a simple explanation for the slow convergence (resolved radius  $\propto N^{-1/3}$ ) in density profiles of CDM haloes simulated at different resolutions (Moore et al. 1998; Ghigna et al. 2000).

(ix) Most of the affected particles become “relaxed” very early and within the first few Gyrs of the evolution of the Universe. This is hardest epoch to accurately resolve in a cosmological simulation since the relative force errors can be large and the densities of forming haloes can be very high.

The high degrees relaxation show that at  $z = 0$  many particles have completely different energies and orbits compared to their evolution in the mean field limit ( $N \rightarrow \infty$ ). Current cosmological simulations cannot model all the subtle dynamics like orbital resonances which can be important e.g. during tidal stripping (Weinberg 1998). But does relaxation also affect the coarse structure of the object, e.g. their density profiles? It is unclear as to how one should interpret these results for the following reason. The highest rates of relaxation are accumulated early during the formation of the

haloes. Once a subhalo falls into a larger system the particles achieve a higher energy and it is not clear that one should accumulate the relaxation timescale in the way that we have done since the final “hot” system may lose the memory of the initial conditions through violent relaxation processes. Indeed, Moore et al. (1999) show that the initial conditions play little role in determine the final gross structure of dark matter haloes.

The technique of accumulating the relaxation times by measuring the local phase density works very well for near equilibrium structures. In some instances, the energies of particles in a cosmological simulation will increase due to the mass increase from merging. From the virial theorem the growth in mass must be accompanied by an increase in velocity dispersion. Thus it is not clear how relaxation at a high redshift propagates to the final time. However we are mainly interested in the structure of the central dark matter halo and the substructure haloes. These are the regions where most effort is going into comparing theoretical predictions with observational data (e.g. Moore 1994; Stoehr et. al 2002).

The velocity dispersion in the substructure haloes actually decreases slowly with time as mass is stripped. On the other hand the velocity dispersion of the central halo increases with time as it grows by merging. We can quantify the decrease in the mean velocity dispersion in subhaloes or the central halo region by extrapolating the particles backwards through time to examine the velocity dispersion in the progenitor haloes. For the galaxy cluster, half of the relaxation is accumulated since  $z = 3$ . We therefore trace all the particles in the central few percent of the cluster back to  $z = 4$  where we find that all the particles lie in the most massive collapsed haloes at that time – the most massive structures at high redshift form the central cluster region through natural biasing. We find that for the central cluster particles,  $\sigma(z = 4)/\sigma(z = 0) = 1.6$ , i.e. the mean dispersion only increases by 60%. Similarly for cluster substructure haloes, the ratio is practically constant through time. For this reason we are confident that the accumulated degrees of relaxation are a good indicator of the true relaxation of the interesting regions within the simulations.

We note that the following thought experiment illustrates a possible way in which relaxation in the first haloes can affect the central structure of the final halo, even though the energies of the particles may have changed over time: The first haloes to form are several relaxation times old and they achieve this in an near equilibrium state. We have demonstrated that our cumulative estimator works very well for non-equilibrium systems that have P.E./K.E. ratios as large as ten times the equilibrium mean (Figure 5). We also show that these first poorly resolved haloes will develop constant density cores through relaxation (Figure 8). Now consider what happens when this halo accretes into a larger system. Because of the constant density core the satellite will completely disrupt at some distance from the centre of the final object (Moore, Katz & Lake 1996). If the accreting halo had a steep cusp resolved with more particles then it may sink deeper within the potential and deposit mass at smaller radii (e.g. Barnes 1999, Syer & White 1998). Thus the early relaxation could affect the final density profile even if the relative energies of the particles were initially quite different from their final energies. Unfortunately, quantifying

this effect and determining if it is at all important is best achieved by increasing the resolution by several orders of magnitude over the haloes simulated in this paper.

This paper has been typeset from a  $\text{T}_{\text{E}}\text{X}/\text{L}^{\text{A}}\text{T}_{\text{E}}\text{X}$  file prepared by the author.

## ACKNOWLEDGMENTS

We thank Adrian Jenkins and Alexander Knebe for helpful suggestions and comments. We also would like to thank the Swiss supercomputing centre at Manno for computing time where many of these numerical simulations were performed.

## REFERENCES

- Barnes J. E., 1999, in Barnes J. E., Sanders D. B., eds, Proc. IAU Symp. 186, Galaxy Interactions at Low and High Redshift. Kluwer, Dordrecht, p. 137
- Bertin G., 2000, Galactic Dynamics. Cambridge Univ. Press, Cambridge
- Bertschinger E., 2001, ApJSS, 137, 1
- Binney J., Knebe A., 2002, MNRAS, 333, 378
- Binney J., Tremaine S., 1987, Galactic Dynamics. Princeton Univ. Press, Princeton
- Chandrasekhar S., 1942, Principles of Stellar Dynamics. Univ. Chicago Press, Chicago
- Fukushige T., Makino J., 2001, ApJ, 557, 533
- Ghigna S., Moore B., Governato F., Lake G., Quinn T., Stadel J., 2000, ApJ, 544, 616
- Hayashi E., Navarro J. F., Taylor J. E., Stadel J., Quinn T., 2003, ApJ, 584, 541
- Hernquist L., 1990, ApJ, 356, 359
- Huang S., Dubinski J., Carlberg R. G., 1993, ApJ, 404, 73
- Jing Y., Suto Y., 2000, ApJ, 529, L69
- Kazantzidis S., Magorrian J., Moore B., 2004, ApJ, 601, 37
- Klypin A., Kravtsov A. V., Bullock J. S., Primack J. R., 2001, ApJ, 554, 903
- Knebe A., Green A., Binney J., 2001, MNRAS, 325, 845
- Kravtsov A. V., Klypin A. A., Khokhlov A.M., 1997, ApJS, 111, 73
- Navarro J. F., Frenk C. S., White S. D. M., 1996, ApJ, 462, 563
- Moore B., 1994, V.370, Nat, 370, 629
- Moore B., Katz N., Lake G., 1996, ApJ, 457, 455
- Moore B., Governato F., Quinn T., Stadel J., Lake G., 1998, ApJ, 499, L5
- Moore B., Quinn T., Governato F., Stadel J., Lake G., 1999, MNRAS, 310, 1147
- Moore B. 2001, In Martel H. & Wheeler J., eds, AIP Conf. Proc. 586, The dark matter crisis, p.73
- Power C., Navarro J. F., Jenkins A., Frenk C. S., White S. D. M., 2003, MNRAS, 338, 14
- Quinlan G. D., 1996, New Astronomy, vol. 1, no. 3, 255
- Spitzer L., 1987, Dynamical Evolution of Globular Clusters. Princeton Series in Astrophysics, Princeton
- Stadel J., 2001, PhD thesis, U. Washington
- Stoehr F., White S. D., Tormen G., Springel V., 2002, MNRAS, 335, L84
- Syer D., White S. D. M., 1998, MNRAS, 293, 337
- Theis C., 1998, A&A, 330, 1180
- Weinberg M. D., 1998, MNRAS, 297, 101